



Magnetically driven shape memory alloys

J. Enkovaara^a, A. Ayuela^{a,b,*}, A.T. Zayak^c, P. Entel^c, L. Nordström^d,
M. Dube^e, J. Jalkanen^a, J. Impola^a, R.M. Nieminen^a

^a *Laboratory of Physics, Helsinki University of Technology, Helsinki, Finland*

^b *Donostia International Physics Center (DIPC), Spain*

^c *Institute of Physics, Gerhard-Mercator University, Duisburg, Germany*

^d *Condensed Matter Theory, Uppsala University, Uppsala, Sweden*

^e *Department of Physics, McGill University, McGill, Canada*

Received 15 June 2003; received in revised form 17 October 2003

Abstract

Significant progress has been made both in experimentation and theoretical modelling of the magnetic shape memory (MSM) effect, where magnetic field can induce strains of 10%. The theoretical models used to analyze and interpret the different experiments provide reliable information and insight into the physical changes involved in the magnetically driven shape memory alloys. The aim of this review is to discuss the status of the computational modelling we have done. First, the basic MSM requirements and a brief summary of the experimental results for the prototype material Ni–Mn–Ga are given. Then, in the context of atomic-scale calculations, we focus primarily on the understanding of the structural variants, magnetic anisotropy, and Curie temperatures. Finally, we discuss modelling related to mesoscopic scales where we develop a phase field model for the description of twins.

© 2004 Published by Elsevier B.V.

Keywords: Ferromagnetism; Shape memory; Martensitic transformation; Ternary alloys

1. Magnetic shape memory effect

The phenomenon of magnetostriction where an external magnetic field can change the dimensions of the sample was observed already in 1842 by Joule. In normal ferromagnets such as Fe or Ni the strains associated with the magnetostriction are of the order of $10^{-4}\%$ while materials with exceptionally large magnetostriction, for example Tb–Dy–Fe alloys (Terfenol-D), show strains of the order of 0.1% [1]. In contrast, MSM materials can show magnetic field induced strains of 10% [2]. Not only are the strains in the MSM effect two orders of magnitude larger, but also the mechanism is different from ordinary magnetostriction. While ordinary magnetostriction is observed in structurally homogeneous samples, the MSM effect requires a special microstructure. This microstructure is provided by a martensitic transformation. The martensitic transformation [3,4] is a displacive, diffusion free structural transformation from a higher sym-

metry structure (austenite) to a lower symmetry structure (martensite) upon cooling. For example, in Ni₂MnGa the high symmetry phase is cubic while the lower symmetry phase can be tetragonal or orthorhombic. In order to minimize the total shape change (and the macroscopic strain energy) over the whole sample, some microstructure develops in the martensitic phase. A common way to create this kind of microstructure is twinning; because there are usually several crystallographically equivalent ways to deform the high symmetry structure, the deformation may take different directions in different regions of the sample. These structural domains have well defined boundaries and they are called twin variants. A schematic example of the twinning is seen in Fig. 1.

Twin boundaries are often mobile which is exploited in the temperature driven shape memory effect [5]. Due to the easy movement of the twin boundaries the sample can be deformed easily in the martensitic phase. When the material is heated back to the austenitic phase the sample will recover to its original shape, i.e. it will “remember” the shape it had before cooling. Even though strains in the temperature-driven shape memory effect can be several percent, the heat-

* Corresponding author. Tel.: +358-9451-3101; fax: +358-9451-3116.
E-mail address: aay@hugo.hut.fi (A. Ayuela).

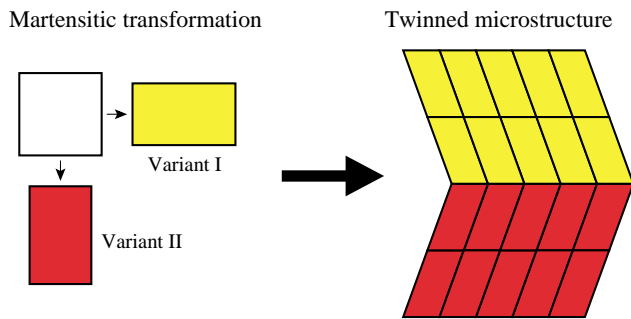


Fig. 1. Schematic illustration of the martensitic transformation and twinning in two dimensions.

ing and especially the cooling are relatively slow processes. Therefore a way to drive the shape change with a faster response would be desirable for many applications. This can be achieved by taking the magnetic degrees of freedom into play.

Magnetic materials such as ferromagnets, antiferromagnets and ferrimagnets are characterized by local magnetic moments. Also, in the absence of an external magnetic field their magnetisation has a certain preferable direction with respect to the crystal lattice, the so-called easy direction. If the easy direction is parallel to the twin direction, then in a twinned microstructure the lattice orientations of the twin variants are different and therefore the magnetisation directions also differ, as shown in Fig. 2a. When an external magnetic field is applied, the magnetic moments try to align in the field direction. If the energy required to rotate the magnetisation out of the easy direction, the magnetic anisotropy energy MAE, is higher than the energy required to move a twin then, it is energetically more favourable to move the twin boundaries instead of rotating the magnetization. The fraction of twins where the easy axis is in the direction of the field will grow at the expense of the other twin variants. This process results in large shape changes as shown schematically in Fig. 2b.

Based on the above discussion the basic requirements for the appearance of the MSM effect can be summarised:

- The material should be (ferro)magnetic and exhibit a martensitic transformation.
- The magnetic anisotropy energy must be higher than the energy required to move a twin boundary.

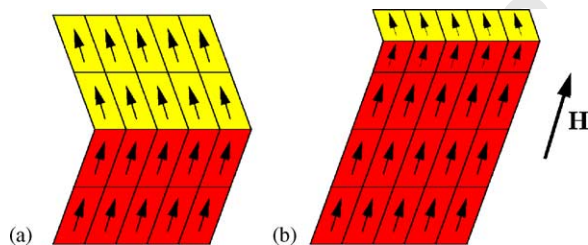


Fig. 2. (a) Magnetic moments without the external field. (b) Redistribution of the variants in an applied field.

From the point of view of practical applications the material should be in the martensitic phase at room temperature. The strength of the required external field depends on the local magnetic moment of the material, so the magnetic moment should be high.

At the moment, the MSM effect has been observed in Fe-Pd [6], Co-Ni-Ga [7], La-Sr-CuO₄ [8] and Ni-Mn-Ga [2,9,10] alloys. La-Sr-CuO₄ is interesting as it is not a ferromagnet but an antiferromagnet, confirming that the magnetic anisotropy is more important than the macroscopic magnetic moment. For practical applications the most promising material is Ni-Mn-Ga. As most of the work presented here concerns Ni-Mn-Ga, some of its experimentally known properties are reviewed next.

2. Experimental studies of Ni-Mn-Ga

Numerous studies of Ni-Mn-Ga alloys have appeared in recent years. Here, a brief summary of the experimental results is given, concentrating on the properties which will be discussed from the theoretical point of view later on.

At the martensitic phase transformation, energy is released or absorbed, and this can be measured by differential scanning calorimetry (DSC). Also, the response to the external magnetic field changes at the transition, allowing the phase transformations to be observed in magnetic susceptibility measurements. These methods allow detection of the occurrence of the transformation and determination of the corresponding temperatures. The advantage of the magnetic susceptibility is that the Curie temperature is also observed clearly as the susceptibility changes from the ferromagnetic to paramagnetic order. On the other hand, DSC measurements allow the energetics of the transition to be studied. Some examples of these measurement are shown in Fig. 3.

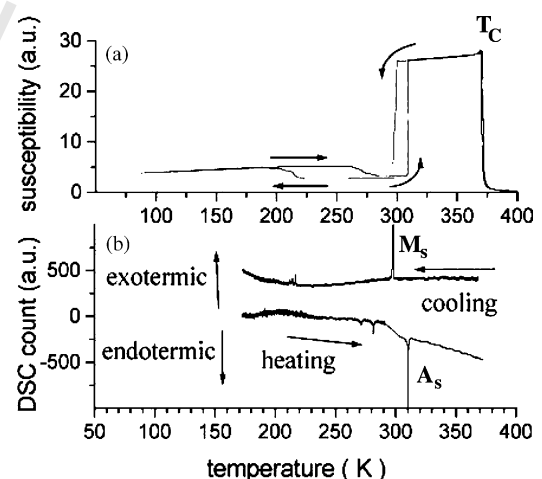


Fig. 3. Examples of (a) magnetic susceptibility and (b) differential calorimetry, showing the martensitic and austenitic transformation temperatures M_s and A_s and the Curie temperature T_C . Courtesy of Heczko [11].

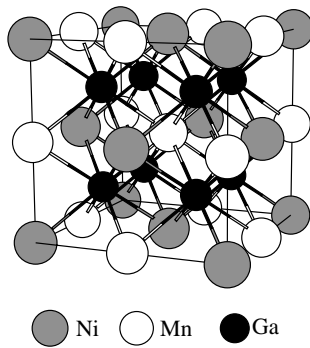


Fig. 4. Cubic $L2_1$ structure with atomic positions of the stoichiometric composition.

124 The martensitic transformation temperatures span over
 125 a wide range, from 160 to 620 K [12–16] and they vary
 126 strongly with composition as a $\sim 1\%$ change in the compo-
 127 sition can alter the transformation temperature by 50° . In
 128 addition to the austenite–martensite transformation, up to
 129 two intermartensitic transformations can be observed. The
 130 Curie temperature is less sensitive to the composition and it
 131 is between 320 and 380 K [12,17,18].

132 The crystal structures of the different phases can be stud-
 133 ied with X-ray and neutron diffraction. The high temperature
 134 austenitic phase has the cubic $L2_1$ structure which is shown
 135 in Fig. 4, with a lattice constant $a_{L2_1} = 11.01$ a.u. [18,19].
 136 This structure has the fcc Bravais lattice with a four atom
 137 basis. As the constituent atoms have similar atomic num-
 138 bers it can be difficult to distinguish them from the X-ray
 139 data. In this case the structure can be interpreted as a bcc
 140 structure with a lattice constant half from that of the fcc
 141 lattice.

142 Three different martensite structures are observed. Two
 143 of them have a basic tetragonal symmetry and one has an
 144 orthorhombic symmetry. In the first tetragonal structure the
 145 ratio of the c and the a lattice constants is $c/a \sim 0.94$ [18].
 146 In addition, there is a shuffling of the atomic planes. The
 147 $(1\bar{1}0)$ planes show a modulation in the $[110]$ direction
 148 with a period of five atomic planes and the structure can
 149 be designated as 5M [15,20]. The other tetragonal structure
 150 has the deformation $c/a \gtrsim 1.2$ and it can be denoted as
 151 non-modulated (NM) because there is no modulation of the
 152 atomic planes [15,21,22]. The orthorhombic structure has
 153 the lattice constant ratios $b/a = 0.94$ and $c/a = 0.89$ and
 154 it is designated as 7M since it has a seven layer modula-
 155 tion similar to the other tetragonal structure [2,11,15,23].
 156 The volume remains approximately constant during all the
 157 transformations.

158 The first martensite which appears on cooling depends
 159 on the composition, but the stability of the structures i.e.
 160 the order in which they appear on cooling seems to be al-
 161 ways the same. This is shown schematically in Fig. 5a. The
 162 NM structure is the most stable before the 7M structure
 163 [15,21,24]. If the 5M structure is to be observed it is trans-

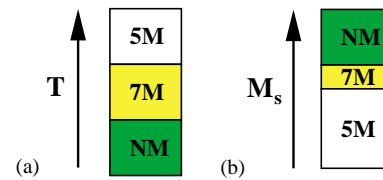


Fig. 5. (a) The stability of the martensitic phases. (b) Relation between the first martensite structure and the transformation temperature M_s .

164 formed directly from the austenite. There is also an em-
 165 pirical correlation between the austenite–martensite trans-
 166 formation temperatures and the first martensite structure as
 167 shown in Fig. 5b [16,25]. The alloys transforming directly
 168 to the NM structure typically have transformation tempera-
 169 tures which can be higher than the Curie point [26,27] and
 170 the 7M phase appears first only in a narrow temperature
 171 range [2,25,28].

172 The lattice constant ratios give the maximum strain which
 173 is available from the twin rearrangement. This limit is 6%
 174 in the 5M structure, 10% in the 7M structure, and more than
 175 20% in the NM structure. Up to now, the maximum strain
 176 has been realised as magnetic-field-induced both in the 5M
 177 [9,29] and in the 7M structures [2]. In the NM structure the
 178 MSM effect has not been observed.

179 As neutrons carry a magnetic moment, neutron diffrac-
 180 tion can provide information about the value of the local
 181 magnetic moments. The total magnetic moment in the sto-
 182 ichiometric composition is found to be $4.1\mu_B$ per formula
 183 unit and it originates mainly from Mn [18,19,30]. Other
 184 experimental tool for the determination of the saturation
 185 magnetisation is the vibrating sample magnetometer (VSM)
 186 also used to obtain the magnetic anisotropy energy. With
 187 VSM one measures the magnetisation as a function of
 188 the external field, as shown in Fig. 6. By applying this
 189 field in different directions with respect to the crystal axis
 190 the magnetic anisotropy energy can be determined as the
 191 area between the two magnetisation curves. The magnetic
 192 anisotropy energy and the easy axis are different for the
 193 particular martensites. In 5M, the $[001]$ direction (the short
 194 c -axis) is the easy axis and the magnetic anisotropy energy
 195 is around 2.0×10^5 J/m³ at room temperature [29,33,34].
 196 In the non-modulated tetragonal structure $[001]$ is the hard
 197 direction and there is an easy plane with an anisotropy
 198 energy of 3.0×10^5 J/m³ [21,32]. In the orthorhombic 7M
 199 structure there are three inequivalent directions. The shortest
 200 axis has the lowest energy, the longest axis the highest en-
 201 ergy and the energy of the intermediate axis is in-between.
 202 The largest energy difference is about 2.2×10^5 J/m³
 203 [2,32].

204 In the following section the above discussed properties are
 205 studied from a theoretical point of view, in some cases also
 206 for other materials than Ni–Mn–Ga. It will be seen that the
 207 calculations can predict and explain with simple arguments
 208 much of the experimentally observed behaviour.

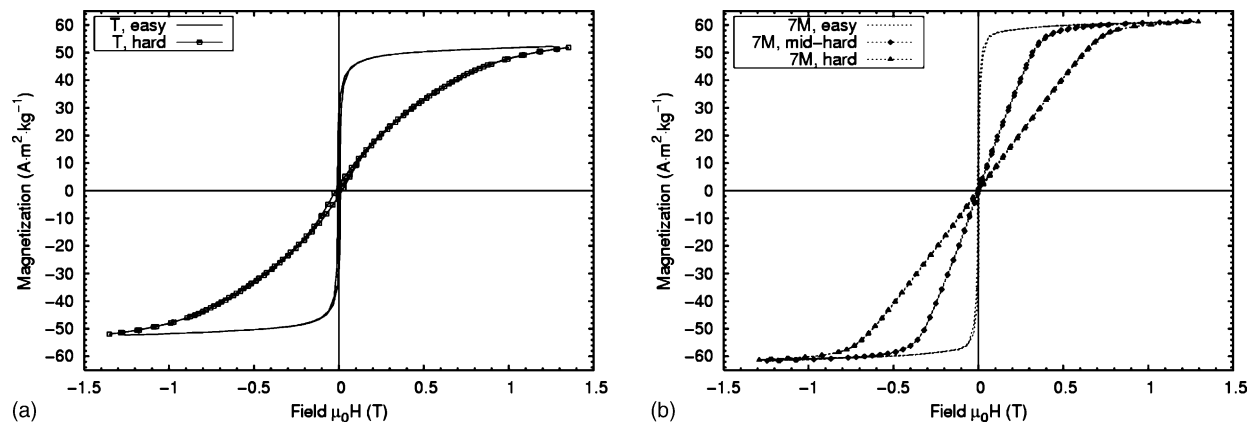


Fig. 6. Magnetisation as a function of the external magnetic field with different field directions in (a) the NM (T in the figure) structure and (b) the 7M structure. Courtesy of Straka [31,32].

209 3. Theoretical results

210 Theoretical work has been done both on microscopic and
 211 mesoscopic scales with a double faceted task. First, we have
 212 a clear mission in trying to understand and interpret the ex-
 213 perimental results in the light of the basic theoretical prin-
 214 ciples. The second task is to motivate new experiments so
 215 that we can increase the understanding necessary for further
 216 progress. Next we give some results about the points that
 217 arose during the last years of studies.

218 3.1. Atomistic calculations

219 All the conclusions presented in this subsection have been
 220 obtained by first principles atomistic calculations within the
 221 density functional theory (DFT). We will refer to the corre-
 222 sponding publications for further details. As said before, a
 223 required property of these materials is that they show local
 224 magnetic moment, which gives the possibility to obtain the
 225 magnetic shape memory effect in them. In a brief course to
 226 atomic magnetism, there are two main quantities that de-
 227 scribe most of the magnetic properties. The first parameter
 228 is the exchange which is connected with the magnetic mo-
 229 ment, and implicitly considered always in this section un-
 230 less stated otherwise. The second quantity is the magnetic
 231 anisotropy which is studied later in Section 3.1.2.

232 3.1.1. Structural properties

233 As many properties of these alloys are based on the struc-
 234 ture, a first question to be answered is what are the reasons
 235 which drive them to these structures. By calculating the total
 236 energy for various structures the possible martensitic phases
 237 can be identified as energy minima. In refs. [35,36] several
 238 Heusler alloys have been studied from this aspect concen-
 239 trating in tetragonal and orthorhombic structures. None of
 240 the studied materials show energy minima for orthorhombic
 241 structures, but there are some minima for tetragonal de-
 242 formations. Ni–Mn–Ga alloys show rubber like behaviour be-
 243 cause a tetragonal transformation is allowed in contrast to

244 other Heusler alloys. In Fig. 7 we show the total energy of
 245 the L₂₁ structure of Fig. 4 versus the tetragonal distortion as
 246 measured by the ratio of *c* and *a* lattice constants. There are
 247 minima at *c/a* = 0.94, 1. and 1.25 which correspond to ex-
 248 perimentally observed structures. The appearance of energy
 249 minima is ascribed to the electronic structure which is de-
 250 scribed in further details in refs. [35,36] as band Jahn–Teller
 251 effect. However, the relative energetic depth of the minima is
 252 different from the stability of the martensitic phases shown
 253 in Fig. 5(a).

254 Theoretically, a tetragonal crystal structure is stabilised
 255 around *c/a* = 0.94 with respect to the L₂₁ structure when,
 256 in addition, modulation shuffles with a period of five atomic
 257 planes is taken into account [37]. This is in agreement with
 258 the observed structures in experimental works. The modu-
 259 lation appears to be critically important for stability of the
 260 tetragonal structure with *c/a* < 1. Here it is found that
 261 the optimum amplitudes of the modulation vary in different
 262 atomic planes.

263 The transition from the tetragonal variant with *c/a* > 1 to
 264 the cubic L₂₁ phase is driven by vibrational entropy when
 265 finite temperature effects are included [38]. A more detailed
 266 study about the vibrational properties of the L₂₁ structure
 267 shows a complete softening of the transverse acoustic mode

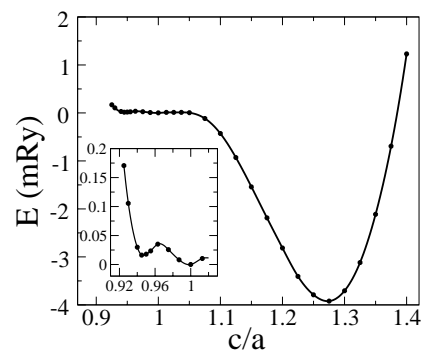


Fig. 7. Total energy of Ni₂MnGa as a function of the tetragonal distortion.

268 has been found around the wave vector $q = 0.33(2\pi/a)$
 269 along the $[110]$ direction [39]. The softening of this
 270 TA_2 phonon mode leads to the premartensitic modulated
 271 super-structure which is observed also experimentally. Fur-
 272 ther phonon anomalies, related to other structural transfor-
 273 mations in Ni_2MnGa , have also been found and examined.
 274 However, these anomalies appear to be due to the coupling
 275 of particular acoustic and optic phonon modes.

276 Some microstructures can also be studied because they
 277 are accessible with the actual computing power. We have
 278 simulated here a $[110]$ twin in the atomistic scale for the
 279 variant with $c/a \sim 0.94$. Preliminary results from this sim-
 280 ulation give a twin formation energy of 31 mJ/m^2 , which is
 281 between the ones in Ni and Cu.

282 3.1.2. Magnetic order

283 We are interested here in the coupling between the mag-
 284 netism and the lattice which is described by the magnetic
 285 anisotropy energy. Some dependences for the magnetic
 286 anisotropy energy have been drawn in Fig. 8 described in
 287 ref. [38,40] in more detail. Around $c/a = 1$, the magnetic
 288 anisotropy in Fig. 8(a) follows mostly a linear trend and
 289 changes its sign. Also the angular dependence shows an
 290 almost perfect uniaxial behaviour as shown in Fig. 8(b).
 291 However, there can be several twins in the martensitic phase
 292 which may complicate the interpretation of the experiments.
 293 Simple estimate for this effect is obtained by averaging
 294 over two twins whose easy axes are perpendicular to each
 295 other [38]. This enables us to explain the puzzling experi-
 296 ments in ref. [41] which reports values for the anisotropy
 297 constants $K_1 = -1.3\mu\text{eV}$ and $K_2 = 1.1\mu\text{eV}$. According
 298 to our interpretation this points clearly to an average over
 299 different twins with $K_1 = 179\mu\text{eV}$ and $K_2 = 1\mu\text{eV}$ which
 300 is in agreement with other experiments.

301 A ferromagnetic material loses its long range magnetic
 302 order and becomes paramagnetic at the Curie temperature.
 303 This temperature is therefore one of the key parameters de-
 304 termining the operation range of the MSM effect. From a
 305 more fundamental point of view the Curie temperature is a

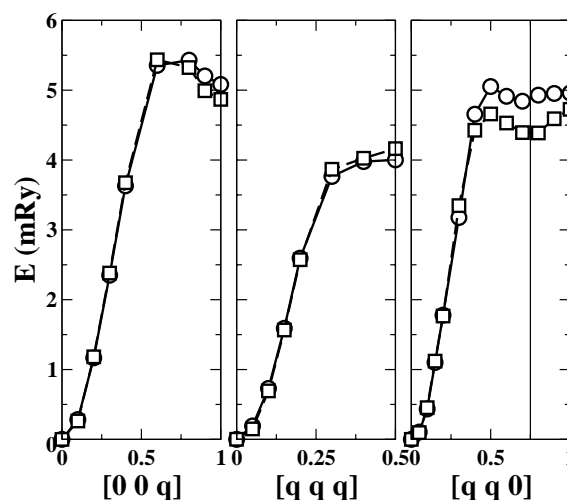


Fig. 9. Total energy as a function of the spiral vector q in the units of $2\pi/a$. (○) Ni_2MnAl , (□) Ni_2MnGa .

306 basic property for the theoretical understanding of a ferro-
 307 magnetic material. The decrease of macroscopic magnetisa-
 308 tion with increasing temperature is caused by longitudinal
 309 and transverse fluctuations of magnetic moments. It is as-
 310 sumed that transverse excitations of magnetisation are the
 311 dominant origin for the Curie temperature in transition met-
 312 als because large local magnetic moments are shown to
 313 exist above the Curie point [42,43]. These transverse excita-
 314 tions are quantised as magnons. In ref. [44] the magnon re-
 315 lated properties of Ni_2MnGa and Ni_2MnAl are studied with
 316 total-energy calculations of spin spirals. The spin spiral is
 317 a magnetic configuration where the magnetisation direction
 318 varies with a well-defined period. The period is determined
 319 by the wave vector q . The total energy as a function of the
 320 spiral vector q is shown in Fig. 9 for the high symmetry
 321 directions $[001]$, $[111]$ and $[110]$.

322 It is seen that the energies are very similar both in
 323 Ni_2MnGa and in Ni_2MnAl . For small values of q the en-
 324 ergy grows quadratically, but the dispersion flattens for

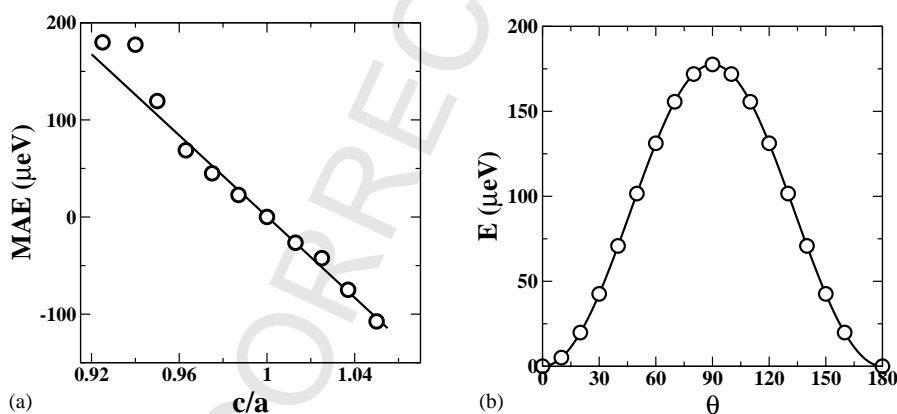


Fig. 8. Magnetic anisotropy energy as function of the tetragonal distortion c/a (a) and of the magnetisation direction θ (b).

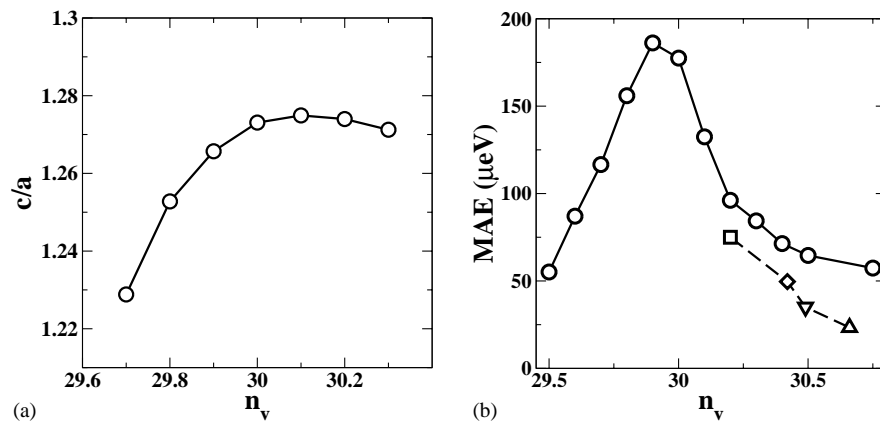


Fig. 10. (a) Tetragonality and (b) the MAE for $c/a = 0.94$ as a function of the number of valence electrons n_v . The stoichiometric composition corresponds to $n_v = 30$. Experimental values from (\square) ref. [34], (\diamond) ref. [29], (\triangle) ref. [46].

larger q especially in the [1 1 0] direction. The theoretical spin wave stiffness D obtained from the total energies, $\omega_q = Dq^2$, shown in Fig. 9 is $D = 77 \text{ mRy a.u.}^2$ and it is in good agreement with the experimental value of 79 mRy a.u.^2 measured in Ni-Mn-Ga films [45]. Also the Curie temperature can be estimated from the calculated energy dispersions in Fig. 9 [44]. We obtain the Curie temperature 480 K in good agreement with the experimental one 380 K .

3.1.3. Role of composition and ageing process

It was clear on the first steps of this research that the key properties of these alloys showed a marked composition dependence. At a first step the composition dependence can be studied within the rigid band approach which considers only the change in the number of valence electrons. As seen in Fig. 10(a), the c/a ratio changes in an appreciable way for the variant with $c/a > 1$. The experimental trend of decreasing MAE with increasing electron concentration is reproduced also by the rigid band approximation

as seen in Fig. 10(b). The inclusion of electronic structure is needed in order to explain these trends, for details see Refs. [38,40].

In ref. [47] we have gone beyond the rigid band approximation and studied the alloying effects with supercell calculations of $\text{Ni}_2\text{Mn}_{1.25}\text{Ga}_{0.75}$. Experimentally, compositions close to $\text{Ni}_2\text{Mn}_{1.25}\text{Ga}_{0.75}$ have good MSM properties as large strains are obtained around room temperature. This composition is obtained by replacing one Ga atom by an Mn atom in the 16-atom supercell, as shown in Fig. 11(a). The main difference in the supercell approach to the actual experimental composition is that in the supercell the extra Mn atoms are perfectly ordered while in the real material they can be distributed randomly in the Ga sites. The most important result obtained from the calculations is that the magnetic moments of the extra Mn atoms favour anti-ferromagnetic alignment with respect to the neighbouring Mn atoms. The magnetic moment of a Mn atom is approximately a constant $3.5\mu_B$ regardless of the direction of the moment or electron concentration. Hence, the antiferromagnetic order-

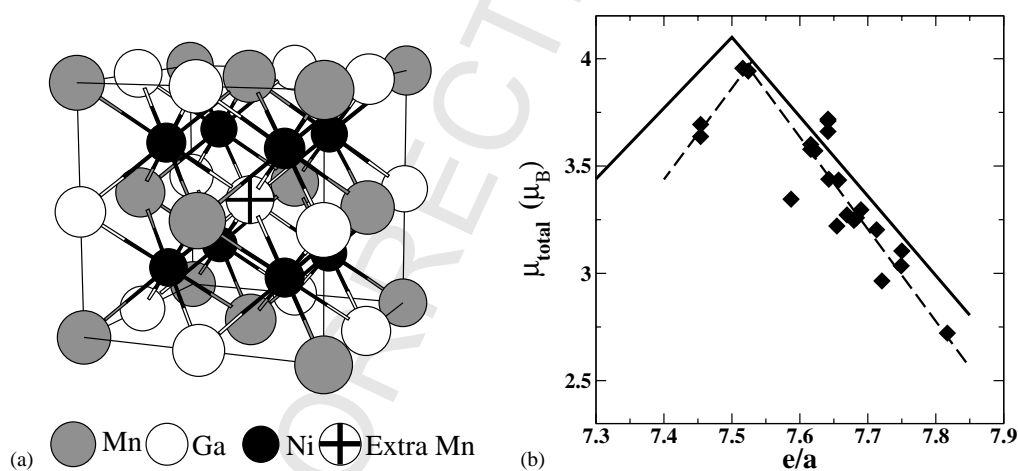


Fig. 11. (a) L2₁ supercell of $\text{Ni}_2\text{Mn}_{1.25}\text{Ga}_{0.75}$. (b) Saturation magnetisation vs. the average number of valence electrons per atom (e/a). The dashed line is a linear fit to the experimental data and the solid line is the theoretical prediction assuming a 50% Ni content.

ing of the extra Mn means that every additional Mn reduces the total moment by $3.5\mu_B$. The magnetic moment of $\text{Ni}_2\text{Mn}_{1+x}\text{Ga}_{1-x}$ can be described with a simple model as $\mu_{\text{total}} = 2\mu_{\text{Ni}} + (1 - |x|)3.5\mu_B$, where the Ni moment μ_{Ni} varies around the stoichiometric value of $0.5\mu_B$ with the electron concentration according to the rigid band results. As seen in Fig. 11(b) the model describes well the experimental variation of the magnetisation. From this agreement it can be concluded that the Mn atoms substituted at Ga sites are antiferromagnetically coupled to the Mn atoms at Mn sites.

The extra Mn has also important consequences for the appearance of the martensitic phases. With the antiferromagnetic alignment, the structure with $c/a = 0.94$ is stabilised and it has 5 meV lower energy per formula unit than the cubic structure. In addition, an energy minimum appears for the orthorhombic structure with lattice constant ratios $c/a \sim 0.93$ and $b/a \sim 0.97$. The energy of the orthorhombic structure is between the energies of the two tetragonal minima, so that the theoretical order of phases agrees with the experimental findings discussed in Fig. 5b of Section 2.

On the other hand ageing has to do with the ordering of atoms between the different sub-lattices present in the compounds [48]. A basic ordering process is the atomic exchanges involving only two atoms. For Ni_2MnGa stoichiometry the Mn–Ga, Mn–Ni and Ga–Ni atomic exchanges constitute the whole spectra to be taken into account. The energetically most favourable exchange pair corresponds to Mn–Ga sublattices with an energetic cost of about 1000 K per-formula-unit. This energy difference is in agreement both with the annealing temperature for the thermal treatment in the experimental samples as well as with the onset of disorder phases [49]. These results encourage further experiments. An example is the measurement of saturation magnetic moment before and after thermal treatment, because the Mn atom in the Ga sites align antiferromagnetically when large Mn–Ga disorder is present. Also it seems interesting to look at the change, induced by local order, of the X-ray peaks during ageing.

3.2. Mesoscopic modelling

Based on our previous atomistic results we proposed a Ginzburg–Landau model to describe the behaviour of a twin under a magnetic field for the case of Fig. 12(a). Our expression for the free energy is given by:

$$f = f[e] + f[\theta] + f[e, \theta] + c(\nabla e)^2 + d(\nabla \theta)^2 \quad (1)$$

and in more detail when $c = d = 0$ as for the homogeneous phase,

$$f = \frac{a}{2}e^2 - \frac{e^4}{4} + \frac{e^6}{6} - h\mu \cos(\theta) + k_a p(e) \sin(\theta) \quad (2)$$

where as in refs. [50,51], the relevant order parameter in one dimension is the strain e , and we add also the angle θ of the magnetic moment with the applied field. This model includes: (i) in the three first terms $f[e]$ an elastic contribution together with the magnetic contribution due to strain, which can be fitted to curve of Fig. 7 in the $c/a < 1$ region. (ii) in the magnetic part the interaction with the field (Zeeman term), $f[\theta]$, and (iii) in the so called magnetoelastic part the rotating cost of the magnetic moment $f[e, \theta]$. In the following the magnitude of μ is considered together with the field, and is dropped to $\mu = 1$. In (iii) the turning cost is given by the anisotropy energy that depends on the uniaxial anisotropy constant k_a and the strain in a linear way around $c/a = 1$. With these order parameters we construct several models for the term $p(e)$ involving the magnetic anisotropy and the strain, which can be fitted to linear or higher order polynomials around $c/a \sim 0.94$ variant from the data given in Fig. 8.

Anyhow, upon application of a magnetic field, the variants around a twin boundary become non-equivalent, because one of them will rotate its magnetic moment, as seen in the horizontal regions of Fig. 12(b). This asymmetry will have also consequences around the twin, for instance in the twin shape after certain time of applying the field. For large enough values of the uniaxial magnetic anisotropy, and the magnetic field the variants can become so asymmetric that the so-called Zeeman energy becomes equal to

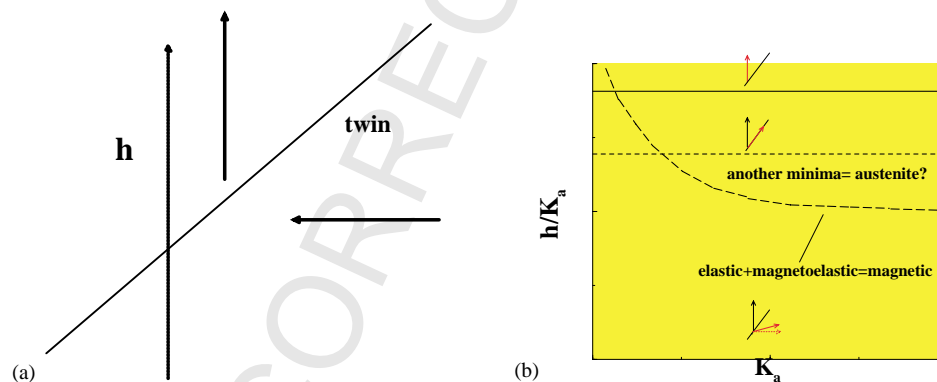


Fig. 12. (a) Twin scheme. (b) Different regions in the order parameter diagram as function of field h and anisotropy constant K_a (see text).

437 the other energetic terms, long dashed line in Fig. 12(b).
 438 In such case a more structured twin can appear, which can
 439 give rise to the nucleation of other phases in more complex
 440 models.

441 Our actual code is ready to deal with microstructures in
 442 two dimensions where following ref. [50] the elastic com-
 443 patibility conditions have been included. Here the analy-
 444 sis of twin patterns will allow us to address a new kind of
 445 problems.

446 4. Conclusions

447 In this review, simulations for magnetic shape memory
 448 alloys are presented. On the atomistic level, structural prop-
 449 erties and phonon dispersions as well as magnetic properties
 450 such as magnetic anisotropy energy and Curie temperature
 451 are described accurately. We are also able to identify the
 452 basic mechanisms behind these properties.

453 Some conclusions about the role of constituent atoms in
 454 stoichiometric Ni₂MnGa can be given. The magnetic mo-
 455 ment originates mainly from Mn, but regarding the other
 456 properties investigated here, Ni is more important. This is
 457 related to the fact that most of the electronic states near the
 458 Fermi-level are due to Ni. The Mn-states are at lower ener-
 459 gies making Mn less important concerning both structural
 460 and transition properties as it can be seen in refs. [35,36].

461 The fact of having several elements in order to form
 462 ternary alloys rises the question about the role of the sub-
 463 lattices. This issue brings into attention two new aspects to
 464 be taken into account. First, when we move out of the ideal
 465 L₂₁ stoichiometry, it means that we are doping some of the
 466 sublattices which bring new characteristics for example in
 467 the form of different magnetic orderings. Second, the atoms
 468 can jump between the sites corresponding to different sub-
 469 structures, although the composition remains constant as in
 470 ageing and annealing processes.

471 In addition, superseded to these atomistic effects, the
 472 twins can assemble and form more complicated patterns. At
 473 this point, we require to address this question within longer
 474 length scales beyond the atomistic approach. A phase field
 475 model including both magnetic field as well as elastic and
 476 magnetic parameters has been introduced for the research in
 477 the mesoscopic scale. Last but not least, we wish to remark
 478 that these alloys are promising for industrial applications up
 479 to now.

480 Acknowledgements

481 This work has been supported by the Academy of Finland
 482 (Centers of Excellence Program 2000–2005), by the Na-
 483 tional Technology Agency of Finland (TEKES) and the con-
 484 sortium of Finnish companies (ABB Corporate Research Oy,
 485 AdaptaMat Oy, Metso Oyj, Outokumpu Research Oy), and
 486 by the Graduate School “Structure and Dynamics of Hetero-

geneous Systems” of the German Science Council (DFG).
 Computer facilities of the Centers for Scientific Computing
 (CSC) Finland and Research Centre Juelich are greatly ac-
 knowledged.

References

- [1] A.E. Clark, in: E.P. Wohlfarth (Ed.), *Ferromagnetic Materials*, vol. 1, North Holland, Amsterdam, 1980, p. 531.
- [2] A. Sozinov, A.A. Likhachev, N. Lanska, K. Ullakko, *Appl. Phys. Lett.* 80 (2002) 1746.
- [3] Z. Nishiyama, *Martensitic Transformation*, Academic Press, New York, 1978.
- [4] D.A. Porter, K.E. Easterling, *Phase Transformations in Metals and Alloys*, Van Nostrand Reinhold, New York, 1981.
- [5] H. Funakubo (Ed.), *Shape Memory Alloys*, Gordon and Breach Science Publishers, London, 1987.
- [6] R.D. James, M. Wuttig, *Philos. Mag.* A 77 (1998) 1273.
- [7] M. Wuttig, J. Li, C. Craciunescu, *Scripta Mater.* 44 (2001) 2393.
- [8] A.N. Lavrov, S. Komiya, Y. Ando, *Nature* 418 (2002) 385.
- [9] S.J. Murray, M. Marioni, S.M. Allen, R.C. O’Handley, T.A. Lograsso, *Appl. Phys. Lett.* 77 (2000) 886.
- [10] K. Ullakko, J.K. Huang, C. Kantner, R.C. O’Handley, *Appl. Phys. Lett.* 69 (1996) 1966.
- [11] O. Heczko, N. Lanska, O. Soderberg, K. Ullakko, *J. Magn. Magn. Mater.* 242–245 (2002) 1446.
- [12] N. Glavatska, I. Glavatsky, G. Mogilny, V. Gavriljuk, *Appl. Phys. Lett.* 80 (2002) 3533.
- [13] V.V. Kokorin, M. Wuttig, *J. Magn. Magn. Mater.* 234 (2001) 25.
- [14] L. Mañosa, A. González-Comas, A.P.E. Obradó, V. Chernenko, A.E.C.V.V. Kokorin, *Phys. Rev. B* 55 (1997) 11068.
- [15] V.V. Martynov, V.V. Kokorin, *J. Phys.* III 2 (1992) 739.
- [16] J. Pons, V.A. Chernenko, R. Santamarta, E. Cesari, *Acta Mater.* 48 (2000) 3027.
- [17] A.N. Vasil’ev, A.D. Bozhko, V.V. Khovailo, I.E. Dikhshtein, V.G. Shavrov, V.D. Buchelnikov, M. Matsumoto, S. Suzuki, T. Takagi, J. Tani, *Phys. Rev. B* 59 (1999) 1113.
- [18] P.J. Webster, K.R.A. Ziebeck, S.L. Town, M.S. Peak, *Philos. Mag.* B 49 (1984) 295.
- [19] P.J. Webster, *Contemp. Phys.* 10 (1969) 559.
- [20] I.K. Zasmichuk, V.V. Kokorin, V.V. Martynov, A.V. Tkachenko, V.A. Chernenko, *Phys. Met. Metall.* 69 (1990) 104.
- [21] A. Sozinov, A.A. Likhachev, K. Ullakko, *Proc. SPIE* 4333 (2001) 189.
- [22] W.H. Wang, G.H. Wu, J.L. Chen, S.X. Gao, W. Zhan, G.H. Wen, X.X. Chan, *Appl. Phys. Lett.* 79 (2001) 1148.
- [23] V.A. Chernenko, C. Segui, E. Cesari, J. Pons, V.V. Kokorin, *Phys. Rev. B* 57 (1998) 2659.
- [24] G. Feng, C. Jiang, T. Liang, H. Xu, *J. Magn. Magn. Mater.* 248 (2002) 312.
- [25] A. Sozinov, in press.
- [26] C. Jiang, G. Feng, H. Xu, *Appl. Phys. Lett.* 80 (2002) 1619.
- [27] V.V. Khovailo, T. Takagi, J. Tani, R.Z. Levitin, A.A. Cherechukin, M. Matsumoto, R. Note, *Phys. Rev. B* 65 (2002) 092410.
- [28] A. Sozinov, A.A. Likhachev, N. Lanska, K. Ullakko, V.K. Lindroos (2002), in press.
- [29] O. Heczko, A. Sozinov, K. Ullakko, *IEEE Trans. Magn.* 36 (2000) 3266.
- [30] P.J. Brown, A.Y. Bargawi, J. Crangle, K.-U. Neumann, K.R.A. Ziebeck, *J. Phys.: Condens. Matter* 11 (1999) 4715.
- [31] O. Heczko, L. Straka, N. Lanska, K. Ullakko, J. Enkovaara, *J. Appl. Phys.* 91 (2002) 8228.
- [32] L. Straka, O. Heczko, *J. Appl. Phys.* 93 (2003) 8636.
- [33] O. Heczko, K. Jurek, K. Ullakko, *J. Magn. Magn. Mater.* 226 (2001) 996.

- 550 [34] R. Tickle, R.D. James, J. Magn. Mater. 195 (1999) 627. 567
551 [35] A. Ayuela, J. Enkovaara, K. Ullakko, R.M. Nieminen, J. Phys.: 568
552 Condens. Matter 11 (1999) 2017. 569
553 [36] A. Ayuela, J. Enkovaara, R.M. Nieminen, J. Phys.: Condens. Matter 570
554 14 (2002) 5325. 571
555 [37] A.T. Zayak, P. Entel, J. Enkovaara, A. Ayuela, R.M. Nieminen, J. 572
556 Phys.: Condens. Matter 15 (2003) 159. 573
557 [38] J. Enkovaara, A. Ayuela, L. Nordström, R.M. Nieminen, J. Appl. 574
558 Phys. 91 (2002) 7798. 575
559 [39] A.T. Zayak, P. Entel, J. Enkovaara, A. Ayuela, R.M. Nieminen, Phys. 576
560 Rev. B 68 (2003) 132402. 577
561 [40] J. Enkovaara, A. Ayuela, L. Nordström, R.M. Nieminen, Phys. Rev. 578
562 B 65 (2002) 134422. 579
563 [41] B.D. Shanina, A.A. Konchits, S.P. Kolesnik, V.G. Gavriljuk, I.N. 580
564 Glavatskij, J. Magn. Mater. 237 (2001) 309. 581
565 [42] A. Kakizaki, J. Fujii, K. Shimada, A. Kamata, K. Ono, K. Park, 582
566 T. Kinoshita, T. Ishii, H. Fukutani, Phys. Rev. Lett. 72 (1994) 583
2781. 584
- [43] E. Kisker, K. Schröder, M. Campagna, W. Gudat, Phys. Rev. Lett. 52 (1984) 2285. 567
[44] J. Enkovaara, A. Ayuela, J. Jalkanen, L. Nordström, R.M. Nieminen, 568
, Phys. Rev. B 67 (2003) 054417. 569
[45] S.I. Patil, D. Tan, S.E. Lofland, S.M. Bhagat, I. Takeuchi, O. Famodu, 570
J.C. Read, K.-S. Chang, C. Craciunescu, M. Wuttig, Appl. Phys. 571
Lett. 81 (2002) 1279. 572
[46] S. Wirth, A. Leithe-Jasper, A.N. Vasil'ev, J.M.D. Coey, J. Magn. 573
Magn. Mater. 167 (1997) L7. 574
[47] J. Enkovaara, O. Heczko, A. Ayuela, R.M. Nieminen, Phys. Rev. B 575
67 (2003) 212405. 576
[48] X. Ren, K. Otsuka, Nature 389 (1997) 579. 577
[49] R.W. Overholser, M. Wuttig, D. A. Neumann, Scripta Mater. 40 578
(1999) 1095. 579
[50] S.R. Shenoy, T. Lookman, A. Saxena, A.R. Bishop, Phys. Rev. B 580
60 (1999) R12537. 581
[51] S. Kartha, J.A. Krumhansl, J.P. Sethna, L.K. Wickham, Phys. Rev. 582
B 52 (1995) 803. 583
584

UNCORRECTED PROOF